Earth and Planetary Science
https://journals.nasspublishing.com/index.php/eps

RESEARCH ARTICLE

Multi-Proxy Environmental Reconstruction of the Covacha de los Zarpazos in Galería Site (Atapuerca, Spain)

Serena D'Arcangelo[1,2*], Fátima Martín-Hernández[2,3,4], Josep María Parés[5], Ana Álvaro Gallo[5], Ana Isabel Ortega[5], Paula García-Medrano[6,7,8,9], Isabel Cáceres[8,9]

1. Istituto Nazionale di Geofisica e Vulcanologia (INGV), Rome, 00143, Italy
2. Department of Physics of the Earth and Astrophysics, Faculty of Physics, Complutense University of Madrid, Madrid, 28040, Spain
3. Geosciences Institute (UCM, CSIC), Madrid, 28040, Spain
4. Institute of Applied Magnetism (UCM), Las Rozas, 28230, Spain
5. Geochronology and Geology, Centro Nacional de Investigación sobre la Evolución Humana (CENIEH), Burgos, 09002, Spain
6. Département Homme et Environnement, Muséum National d'Histoire Naturelle, Paris, 75005, France
7. Department of Britain, Europe and Prehistory, British Museum, London, N1 5QJ, United Kingdom
8. Institut Català de Paleoecologia Humana i Evolució Social (IPHES-CERCA), Tarragona, 43007, Spain
9. Department d'Història i Història de l'Art, Universitat Rovira i Virgili, Tarragona, 43003, Spain

Abstract: Magnetic properties of iron oxides provide invaluable data for environmental reconstruction during sediment deposition. Encouraged by the results of our previous studies in the near Gran Dolina site, we investigate the GI waterlain facies sediments that fill Galería Complex cave (Sierra de Atapuerca, Spain), in particular the Covacha de los Zarpazos cave considering two vertical profiles at different walls and comparing them with two profiles previously analysed. For the first time in this cave, we propose a correlation among these two walls based on the low field susceptibility values. An environmental reconstruction is proposed based on the pedogenesis and weathering processes, and water activity influencing the composition, concentration and grain size of magnetic minerals. In order to have a more comprehensive interpretation, elemental geochemistry was also analysed. The results allow to identify three different sections with the alternation of environmental characteristics.

Keywords: Environmental magnetism; Galería cave; Waterlain facies; Pedogenesis influence; Weathering degree

*Corresponding Author:
Serena D'Arcangelo,
Istituto Nazionale di Geofisica e Vulcanologia (INGV), Rome, 00143, Italy
Department of Physics of the Earth and Astrophysics, Faculty of Physics, Complutense University of Madrid, Madrid, 28040, Spain;
Email: serena.darcangelo@ingv.it

Received: 26 May 2024; **Received in revised form:** 13 June 2024; **Accepted:** 26 June 2024; **Published:** 14 August 2024

Citation: D'Arcangelo, S., Martín-Hernández, F., Parés, J.P., et al, 2024. Multi-Proxy Environmental Reconstruction of the Covacha de los Zarpazos in Galería Site (Atapuerca, Spain). *Earth and Planetary Science*. 3(2): 60–81. DOI: https://doi.org/10.36956/eps.v3i2.1108

DOI: https://doi.org/10.36956/eps.v3i2.1108

1. Introduction

Environmental magnetism (EM) provides invaluable proxies for paleoenvironmental reconstructions based on the measurement of magnetic properties of sediments. Since the beginning of this science, the EM has been successfully applied to lake sediments, loess deposits, deep sea sediments and, in the last decades, also centred on cave sediment despite the difficulty derived by the numerous processes that affect the cave sediment (pedogenesis, erosion, post-depositional deformation, groundwater activity, weathering processes) [1–5]. The basis of the EM is the knowledge of the composition, the concentration and the grain magnetic size of the magnetic minerals present in the samples and, from these data, reconstruct the environmental characteristics and climate variations considering the different processes that could affect the sediments in those conditions. The knowledge of the depositional environment of the sediments and the processes responsible for the formation of secondary magnetic minerals, allows to better understand the interaction of human activity and the environment [6].

From the sedimentological point of view, cave sediment was divided into entrance facies, waterlain facies and interior facies [7]. The entrance facies are composed of deposits a few meters just inside and outside the cave; in which there are different depositional and post-depositional processes from various sources. The waterlain facies represent part of much older phreatic deposits. Underground rivers transport inside the cave clastic sediments similar to fluvial deposits in the open air. These sediments are well sorted in narrow channels, and become finer upward; the sandy component is moderately well sorted with fining and coarsening upward sequences with common interbedding with silts and clays and fine laminated bedding [7]. Moreover, they could present small erosional channels that form cut-and-fill structures and some imbrication shown by the gravels. The erosional processes may continue also in the presence of hominin occupation and such remnants are redeposited as colluvium or solifluction deposits within the cave. The interior facies represent the accumulation of gravity-fall deposits derived from the roof and walls; finer-sized sediments can also be produced by bedrock weathering [7]. The rock fall accumulations vary depending on their location in the cave and the sedimentation rate of finer sediments (both geogenic and anthropogenic). These deposits are accumulated in remote parts of the cave, typically with no fossil content and, due to the dynamic environment of the cave interiors, they represent a series of depositional and erosional events (sedimentary cycles) [7].

Due to the numerous and well-preserved hominin remains of five distinct species (Homo antecessor introduced in this site), the karst of the Sierra de Atapuerca (Figure 1a) is one of the most important archeopaleontological sites for understanding human evolution in Europe during the Early and Middle Pleistocene. For its unique testimony of hominins evolution, this archaeological site was added to UNESCO's World Heritage List in 2000 (https://whc.unesco.org/en/list/989/).

We focus on the Galería Complex site, in detail on the Covacha de los Zarpazos cave, dated on 500–250 ka [8–14]. Due to the phreatic/vadose conditions in this cave [15], its paleoenvironmental reconstruction needs to consider different processes that affect the magnetic properties of cave sediments: pedogenesis, weathering, and water activity.

A previous study [5] centred on the Galería section documented the presence of three main components on the magnetic signal: the magnetite and the fine-grained antiferromagnetic minerals, hematite and goethite, of pedogenic origin. Since the pedogenesis processes lead to the preferential formation of hematite over goethite, the variation of goethite versus hematite may be considered a proxy for the degree of soil maturity [16]. Since the organic matter and iron-reducing bacteria may foment, during pedogenesis, a local reducing environment, favourable to the reduction of hematite to magnetite and subsequent oxidation to maghemite [17], the goethite/hematite ratio may be considered as a proxy of climatic deterioration. On the other hand, the elemental geochemistry analysis may suggest the degree of weathering and pedogenesis processes, as explained by reference [18]. Finally, the water activity variations were observed on the anisotropy of magnetic susceptibility in Galería site [19].

This paper pretends to propose a paleoenvironmental reconstruction based on these different factors (pedogenesis, weathering and water activity) that affect the waterlain deposits in Covacha de los Zarpazos analysing four profiles: two, GA1 and GA3, located in the NE wall and other two, GA2 and GA4, in the NW wall (Figure 2). All the profiles are in stratigraphic connection and at a short distance, allowing a stratigraphic correlation among these walls taking into account the inclination of the strata towards SW and on the basis of the low field susceptibility. The results thus shed light on the correlation of the magnetic signals with the development of climatic conditions, the hydrological changes of the groundwater river responsible for deposition of the waterlain facies and post-depositional weathering processes.

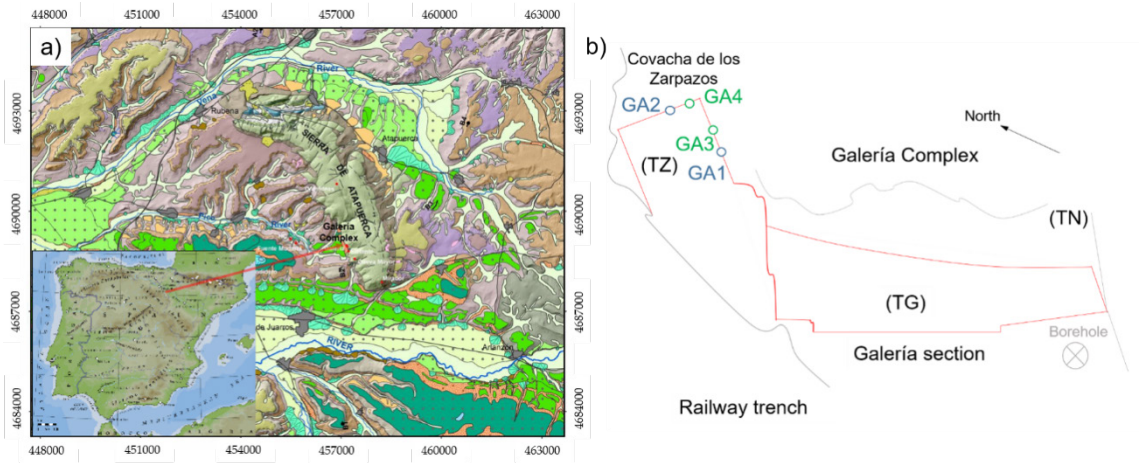

Figure 1. Location of the archaeological site in the Sierra de Atapuerca. (**a**) Geomorphological map of the Sierra de Atapuerca, with Galería Complex highlighted. (**b**) Section of Galería Complex with the position of profiles analysed in Covacha de los Zarpazos and borehole at the entrance of Galería section. The red lines represent the exposed sediments and the grey one the limestone wall; following the reconstruction proposed by reference [15].

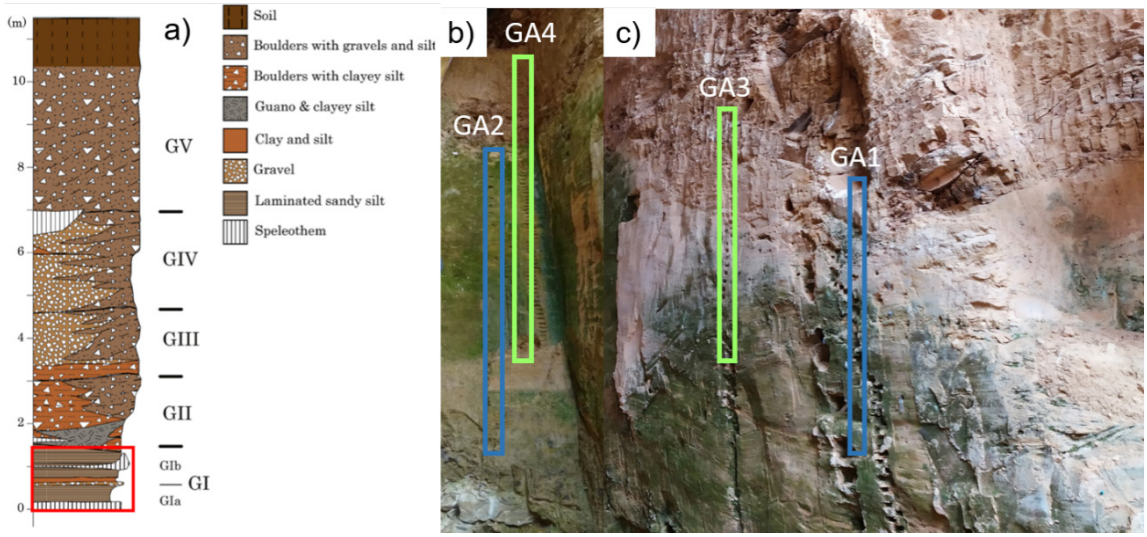

Figure 2. Details of the facies analysed, with the respective profiles considered. (**a**) Galería stratigraphic column, with indication of the analysed interval shown as a red rectangle (modified from reference [15]); (**b**) Detailed view of the NW wall, with profiles GA2 and GA4. (**c**) Detailed view of the NE wall, with GA1 and GA3 profiles.

2. Geological setting

Sierra de Atapuerca karst is divided into three sub-horizontal levels, formed in the Late Cretaceous limestones and dolostones in relation to the evolution of the middle Arlanzón River [20,21]. The intermediate level (approx. 995 m a.s.l.) includes, among others, the "Trinchera del Ferrocarril" (Railway Trench). Among the caves in the Trinchera, the waterlain facies of cave sediments were found only in the lowest part of the Gran Dolina site and Galería Complex [22,23] and, on the basis of 2D and 3D ERT imaging, a conduit was proposed to connect them [24]. The waterlain facies of the Gran Dolina cave were studied for chronologic study [25], for a stratigraphic and sedimentological reconstruction [26] and also an environmental reconstruction was proposed in our previous study [1]. In the waterlain facies of the Galería Complex, only a recent study [15] provides a detailed reconstruction of depositional environments of its sequence.

Galería is a complex sedimentary sequence (section represented in Figure 1b) characterised by strong lateral lithological variations and three separate conduits (sub-sections) that contributed to its sedimentary infilling: Covacha de los Zarpazos (TZ) to the north, Galería itself (TG) in the centre — the main sub-hor-

izontal gallery, and vertical shaft (TN), northernmost infill segment of the neighbouring Tres Simas cavity, located at the southern end of the Galería site [20,27]. Studies focused on the lithic assemblage and faunal remains suggest the use of this cave as a marginal area for knapping activities and sporadic visits in pursuit of animal resources, providing interesting information to reconstruct the occupational pattern of the entire Sierra de Atapuerca [28–31]. In addition, at the entrance of Covacha de los Zarpazos, in the upper sedimentary units, a human mandibular fragment and a cranial fragment were found [32]. The entire sedimentary sequence of Galería is composed of fluvial sediments; probably coming from the southern contact between the Sierra de Atapuerca with the Arlanzón River [15,21].

A recent environmental magnetism study in TG [5] documented a pedogenic origin of magnetite concentration and proposed the goethite presence as a proxy for climate-stratigraphic correlation at Galería since its fluctuating values may be due to alternating humid and dry conditions.

The Galería Complex is constituted of five main filling units (from GI to GV, from base to top) and one paleosoil GVI [22]. The cave is dated by different methods in previous studies [8–9,10,12]; as a result, the timeframe of the cave is between 500 ka and 250 ka. GI unit detected the transition from reverse (Matuyama) to normal (Brunhes) polarity (770.2 ± 7.3 ka; critical stratigraphic marker on the definition of Lower-Middle Pleistocene [33,34]), which confirmed a substantial sedimentation hiatus in this lowermost part of the profile in the central part of Galería area [14].

The GI represents a unique sedimentary unit of waterlain sedimentary facies: laminated silts, limestone breccia, and speleothems related to flowing or stagnant waters. At the boundary with GII, a collapse of the roof cave generated the opening at external influence documented in successive entrance facies characterised by gravity flows and erosional processes [35,36]; humid and wooded conditions were proposed for this unit [37]. In the GIII unit, a displacement of the hominin to the TZ area was documented, as a clear consequence of the reduction of the cave environment and the loss of the effective natural tramp; moreover, the presence of trampling suggests dry conditions and a decrease of wooded [31]. These two units, GII and GIII, represent the single fertile sequence of Zarpazos cave: the right adult mandible fragment, assigned to Homo heidelbergensis [38], was found in the GII unit [32], and a neurocranial fragment of an adult human discovered at the base of the GIII unit [39]. The GIV unit presents a merely clastic sedimentation, cold conditions were identified in the GV unit and finally, a maximum warm was testified by a relict soil in the GVI unit [40].

The GI unit is divided into two subunits: GIa and GIb above; evidenced also by sedimentation changes, probably due to changes in hydrological conditions. In Covacha de los Zarpazos, the entire GI sedimentary sequence is affected by soft-sediment deformation structures, including five main faults in the NW wall of the conduct. As evidenced by reference [15], the GIa subunit was deposited during the Early Pleistocene in phreatic or epiphreatic conditions while GIb presents important erosion events and reworking materials during the Middle Pleistocene in vadose conditions. Both units were subdivided into six subunits.

In detail, the lowest subunit of GI, GIa.6, is formed by at least four cycles of dropping in the water table, in epiphreatic conditions. In a vertical discordant boundary succeed the GIa.5 subunit that, composed of sandy silts with some cross-lamination, suggests phreatic conditions inside the cave. The GIa.4—locally deposited only in Covacha de los Zarpazos and absent in the Galería area—indicates an energy drop in the system and less turbid water with respect to the previous subunit. The energy of the environment increases again in the successive sandy silt layer with no clear lamination, GIa.3 subunit, under stable phreatic conditions with water table rise. Some speleothems present in GIa.2 indicate a break in the sedimentation process for a long period in vadose conditions before the last deposit of Early Pleistocene, GIa.1, discordant with the underlying layers and cut by erosion surface. As mentioned before, from the GIb subunit the sedimentation in the Galería Complex changes, passing from mainly epiphreatic to vadose conditions [15].

3.Material and Methods

Four profiles in two different walls of Covacha de los Zarpazos, in stratigraphic connection and at a short distance were studied (Figure 1). A total of 300 non-oriented and unconsolidated samples were collected with standard cubic plastic boxes of 8 cm^3 pushed directly on the outcrop. A rockmagnetic analysis was conducted at the Archaeomagnetism Laboratory at the CENIEH (Burgos, Spain) and at the Paleomagnetism Laboratory at the University Complutense of Madrid (UCM). The magnetic susceptibility parameters represent the first approach in a rockmagnetic study since they provide the concentration of magnetic minerals present. In particular, the low field susceptibility provides an estimation of the ferromagnetic material

present in the samples. The magnetic susceptibility was analysed at CENIEH at two different frequencies (976 Hz and 15616 Hz) with an Agico MFK1-FA Kappabridge, for this first analysis the samples were considered as well as extracted from the cave (mass samples of around 13–14 g). This equipment also provides the phase angle, defined as the difference between in-phase and out-of-phase susceptibility [41,42]. Considering the susceptibility at two frequencies, we are able to consider the frequency-dependence parameter, $\chi_{fd} = 100(\chi_{lf} - \chi_{hf})/x_{lf}(\%)$ as defined by reference [43], where f_{hf} and f_{lf} are high and low frequencies, respectively. Another important rockmagnetic analysis realised is the hysteresis loops measured with a MicroMag 3900 VSM (Vibrating Sample Magnetometer, LakeShore instrument), with a maximum field of 0.5 T. The samples used for this instrument were prepared in small quartz capsules of ~8 ml volume, so the mass sample analysed for this study was around 1 g.

A three-axes SQUID cryogenic magnetometer (SRM, 2G Enterprises) was used to measure the remanent magnetization (natural and anhysteretic, NRM and ARM respectively); the IRM, was performed at 1 T and, in the opposite direction, at 0.3 T; in this case, the samples were disposed in standard 8 cm^3 cubic plastic boxes or in the small quartz capsules used for the VSM. These two measurements consent to calculate the S-ratio (defined by the backward remanence at 0.3 T with the IRM at 1T [44]) and "hard" isothermal remanent magnetization (HIRM, defined as $0.5 \times (IRM_{0.3T} + IRM_{1T})$), quantification of the relative and absolute concentrations, respectively, of antiferromagnetic minerals (hematite and goethite) in mineral mixtures (limits of these parameters exposed in reference [45]). Moreover, progressive IRM acquisition curves up to 1 T were obtained for some selected samples in order to deduce and analyse the different magnetic minerals present through their coercivity using the "Kruiver method" [46]. This method fits the derivate of the IRM acquisition curve in a logarithmic scale into a series of normal distributions characterized by references [46,47]: the saturation isothermal remanent magnetization (SIRM), the median destructive field ($B_{1/2}$), and the width of the distribution half of the maximum intensity (dispersion parameter, DP).

With a view to the magnetic properties, the key ratio for magnetic grain size, IRM_{1T}/χ_{lf}, was used, taking into account its relative limits [48].

The relative concentration of minerals present was obtained by a combination of saturation magnetization (SIRM) of 5 T, reached by an impulse magnetizer (ASC Scientific, Model IM10-30), then an alternating field demagnetization at 100 mT to remove the contribution of any ferrimagnetic minerals and finally a thermal demagnetization at 130 ºC to remove the goethite contribution. The relative contribution of magnetite versus goethite and hematite is obtained by the ratio:

$$\frac{M}{GH} = \frac{SIRM_{5T} - SIRM_{100mT}}{SIRM_{5T}} \quad (1)$$

and the ratio of the relative contribution of goethite versus hematite (as suggested by reference [49]):

$$\frac{G}{H} = \frac{SIRM_{100mT} - SIRM_{130ºC}}{SIRM_{100mT}} \quad (2)$$

It was considered the Day plot ([50] and revisited by reference [51]), by correlating the M_{rs}/M_s with H_{cr}/H_c, obtained by hysteresis loops and back field IRM, to infer the domain state of the iron oxides, and the King plot [52], in order to analyse the relative magnetic grain size of the particles by the slope obtained comparing ARM susceptibility with the low-field susceptibility.

For more complete information about the mineral composition, an in situ analysis was conducted with a portable XRF analyzer NITON Ultra XL3t (manufactured by Thermo Fisher Scientific Inc.) equipped with a 45 mm^2 Silicon Drift Detector (SDD) and an Ag anode of 50 kV. This instrument provides the elements of geochemistry in percentage, to indicate possible post-depositional dissolution of magnetic minerals [3] and elements ratios considered as weathering products [53].

Susceptibility versus temperature curves was acquired at UCM by the CS-3 Temperature Control Unit in connection with the AGICO KLY-4S Kappabridge analysing the susceptibility of minerals in the range from ambient temperature to 700 ºC to discern the magnetic minerals present in the samples from their corresponding Curie temperatures.

4. Results

4.1 Magnetic Composition Analysis

To characterise the relative contribution of the ferromagnetic and para/diamagnetic materials, we analysed the hysteresis loops of all samples (four representatives are shown in Figure 3, mass normalised and corrected for para/diamagnetic contribution, shown in red). There is a strong similarity in the shape of loops belonging to the same profile (Figure 3a,b; Figure 3c,d). In samples from GA1 (Figure 3a,b), we notice

that sample GA1-42 presents a loop slightly more open than GA1-50. Greater contribution of the high coercivity minerals is also observed in samples of GA2 (Figure 3c,d); moreover, the wider loops above and below the middle section reveal the presence of mixtures of minerals with very different coercivity being important for the high coercivity contribution. The para/diamagnetic susceptibility correction has been carried out using the upper branch slope of the curve, despite not being completely saturated.

The thermomagnetic evolution of the susceptibility (Figure 4) up to 700 ºC provides further information about the magnetic mineralogy identifying the Neel/Curie magnetic transitions; red lines indicate the heating while grey lines the cooling. In particular, in the heating of Figure 4a, there is a weak decrease around 500 ºC and an evident decrease at 580 ºC, Curie temperature, T_C, of magnetite in all analysed samples. Figures 4a,b show the cooling curve lower than the heating curve. However, samples from GA2 show a similar higher intensity in the cooling curve (Figure 4c,d). The cooling curve shows the susceptibility values greater than those of the heating; the cooling axis is represented in grey at the right side of the figure. In addition, there is a clear secondary formation of magnetite as evidenced by the increase of the cooling curve between 580–450 ºC and the second weak increase around 300 ºC (Figure 4d). Samples from GA1 display a jump in the susceptibility curve at about 350 ºC indicating the presence of maghemita (Figure 4a,b). In some cases, (Figure 4d) it is possible to distinguish a little decrease of the heating curve at the beginning of the experiment until 120 ºC.

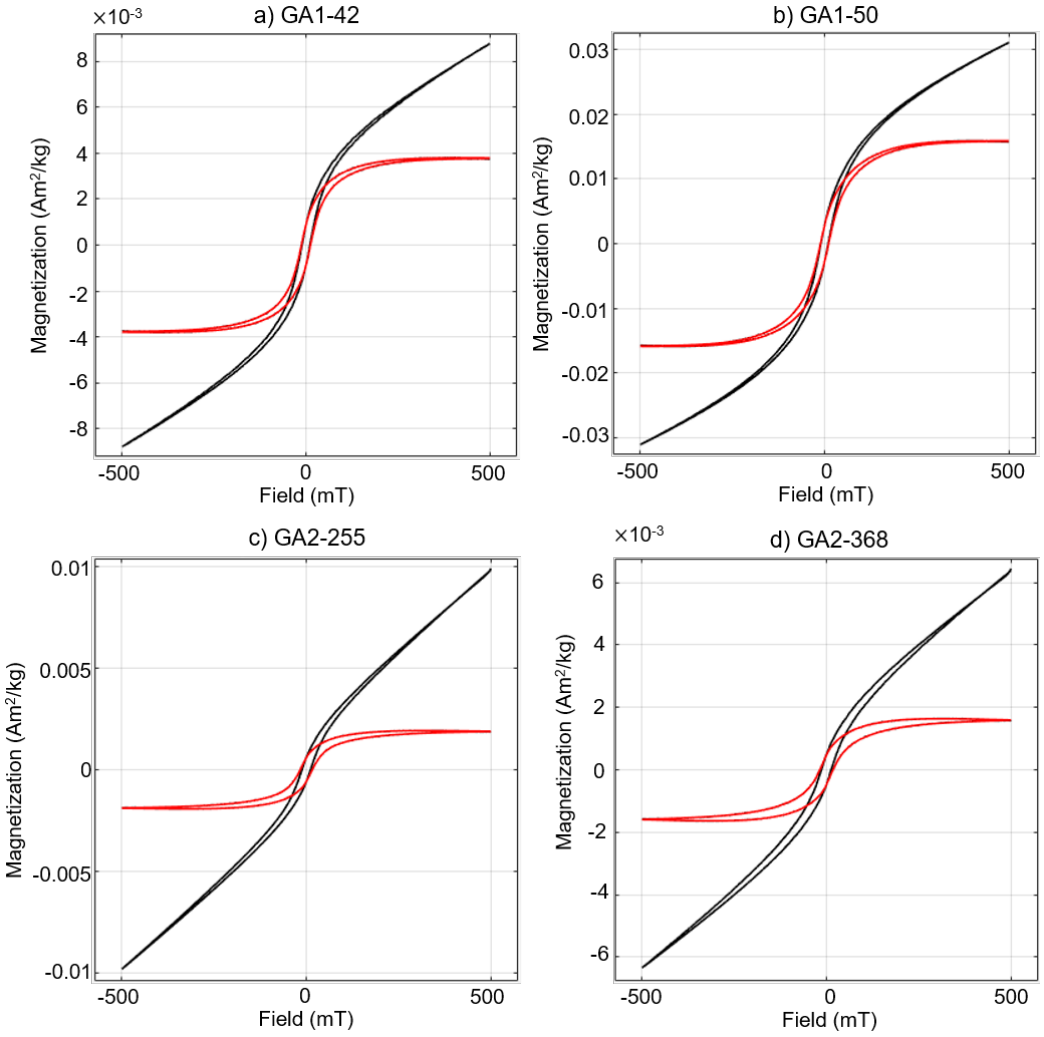

Figure 3. Examples of magnetic hysteresis loops from samples of GA1 and GA2 profiles up to a maximum applied field of 500 mT, mass normalised. The red curves represent subtracting paramagnetic contribution while the black curves represent the hysteresis with paramagnetic contribution. (**a**,**b**) samples from GA1; (**c**,**d**) samples from GA2.

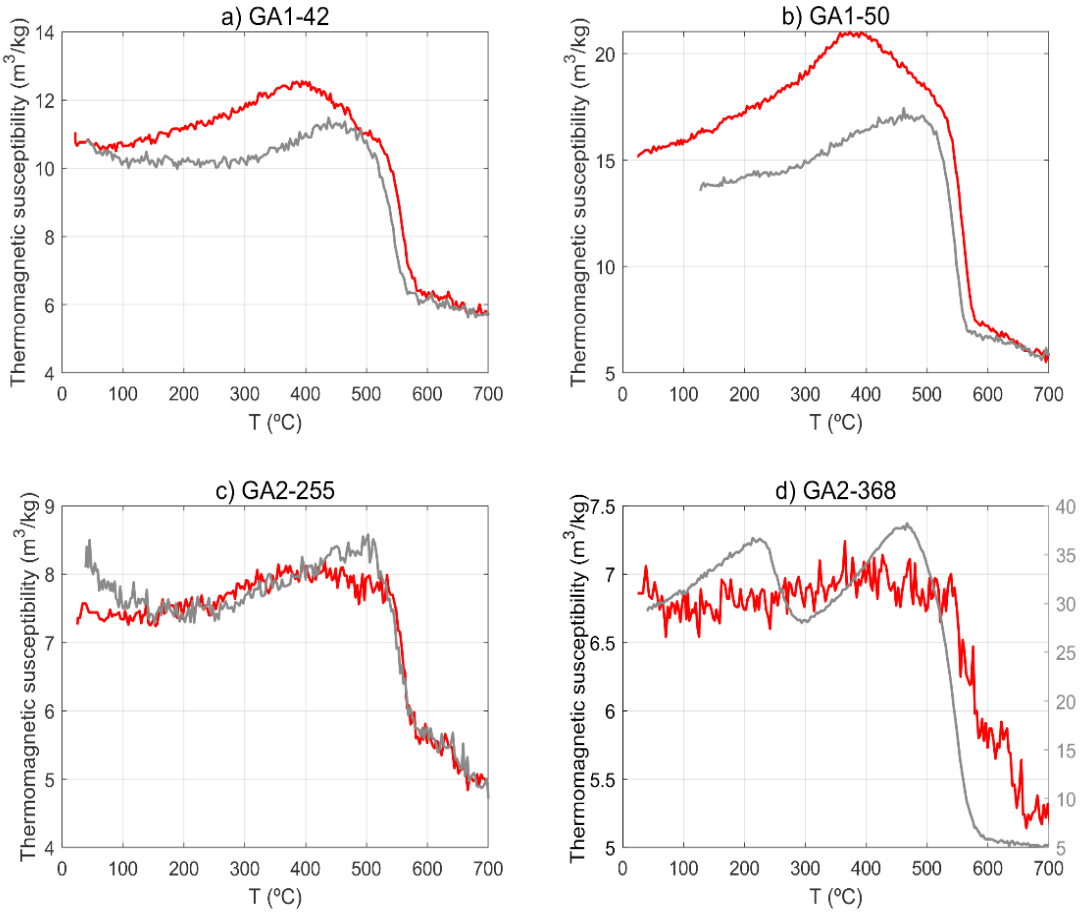

Figure 4. Thermomagnetic curves of the representative samples of GA1 and GA2 profiles. The red line indicates the heating curve while the grey the cooling: (**a,b**) GA1 samples; (**c,d**) GA2 samples. Figure 4d presents the y-axis of the cooling curve at the right side in grey.

From the IRM progressive acquisition curve up to 1 T, normalised by the maximum value (Figure 5), it is possible to distinguish two different distributions of the samples: GA1-43 and GA2-385, samples from the bottom of the profiles, show a rather initial increase, suggesting that a low coercivity phase ferromagnetic fraction in a substantial amount, which very likely is magnetite; while the other two, from the upper part of the profiles (GA1-10 and GA2-360), are dominated by high coercivity component since the saturation was not reached at 1 T (goethite and/or hematite).

The same samples considered for IRM acquisition curves are shown in Figure 6 in order to estimate the difference between non-saturated curves (Figures 6a,c) and semi-saturated ones (Figures 6b,d). Samples are characterized by two-three components of medium, high to medium and high coercivity (Table 1). Samples are characterized by more than one component. Some curves are fitted exclusively by two populations of coercivity of low and mid to high coercivity while others by three. The low coercivity could be identified with magnetite while the medium-high and high could be different proportions of maghemite, hematite and/or goethite [47,54–57]. A summary of the input parameters considered in the modelling of the Kruiver method is shown in Table 1, divided into the different components identified.

4.2 Magnetic Concentration Analysis

Comparing all the profiles analysed, arranged in their spatial disposition and in relation to their depth (Figure 7), it is possible to distinguish three different parts of the entire sedimentary sequence analysed: the top one, on GA3 and GA4 profiles, presents the highest susceptibility values, the bottom one, largely present on GA1 and GA2 profiles, shows greater values of low field susceptibility, and finally a middle section with lower values of susceptibility than others sections. As shown in Figure 7, the different sections are identified with different markers.

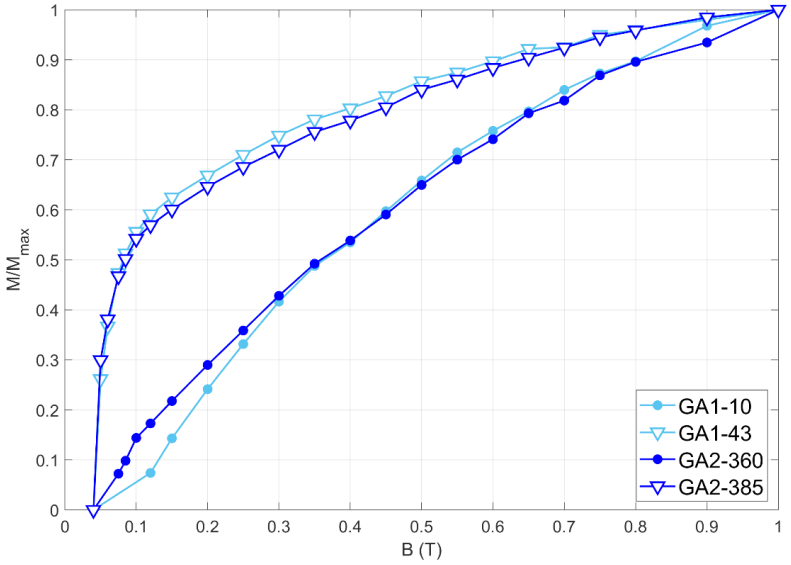

Figure 5. Progressive acquisition of isothermal remanent magnetization (IRM) up to 1 T of two samples of each profile. The resulting curves are normalised by the maximum value.

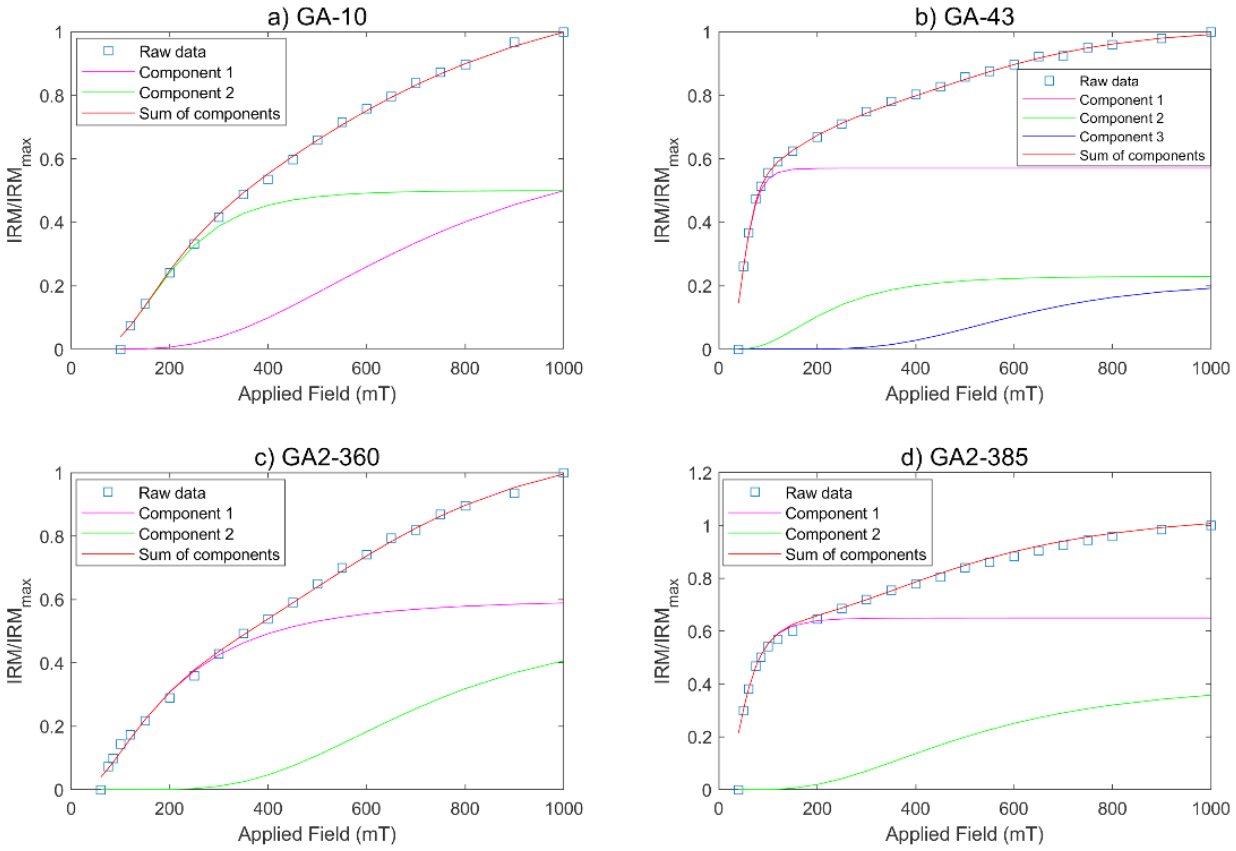

Figure 6. Analysis of the Linear Acquisition Plot (LAP) with the Kruiver approach of the samples illustrated in the IRM progressive acquisition. The squares represent the measured data of the IRM acquisition curve on a linear scale and the solid line is the modelled one (thin lines indicate the components derived from the model). The non-saturated samples of GA1 and GA2 are illustrated in (**a**) and (**c**). The saturated ones of the respective profiles are illustrated in (**b**) and (**d**).

Table 1. Input parameters (SIRM, $B_{1/2}$, and DP) of the model proposed for components individuated for each unit in the Kruiver approach.

Sample	Component 1				Component 2				Component 3			
	SIRM	$B_{1/2}$ (mT)	DP (mT)	IRM (%)	SIRM	$B_{1/2}$ (mT)	DP (mT)	IRM (%)	SIRM	$B_{1/2}$ (mT)	DP (mT)	IRM (%)
GA1-10					5×10^{-1}	200	1.66	43	6.6×10^{-1}	692	1.70	57
GA1-18					6.5×10^{-1}	120	2.00	57	5×10^{-1}	759	1.58	43
GA1-43	5.7×10^{-1}	52	1.51	56	2.3×10^{-1}	214	1.74	23	2.1×10^{-1}	600	1.45	21
GA1-44	7.5×10^{-1}	52	2.00	71					3×10^{-1}	630	1.51	29
GA2-233					5.9×10^{-1}	295	1.82	54	5×10^{-1}	676	1.51	46
GA2-360					6×10^{-1}	195	2.20	55	5×10^{-1}	692	1.51	45
GA2-385	6.5×10^{-1}	52	1.86	62					4×10^{-1}	500	1.74	38

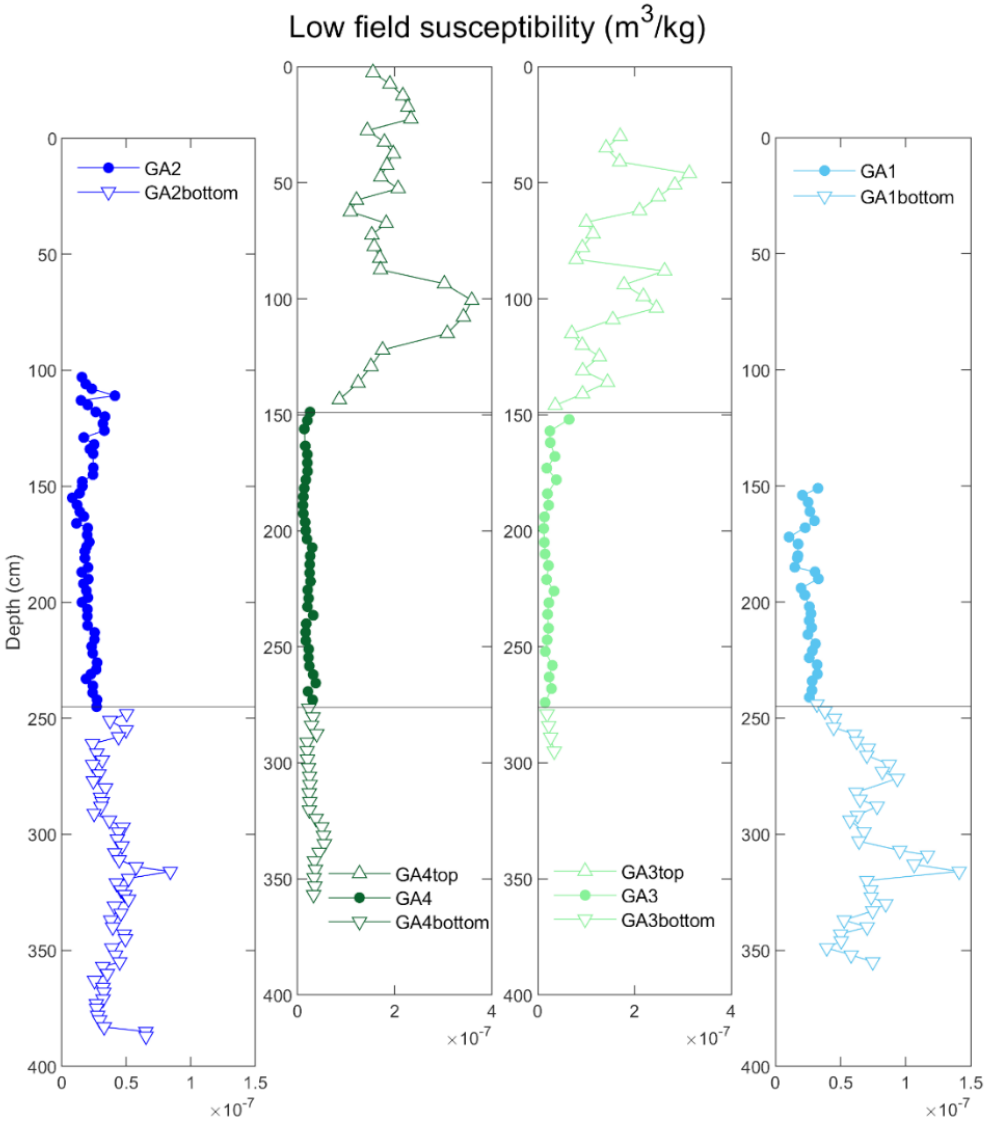

Figure 7. Low field susceptibility of all profiles analysed in the spatial correlation. Note the distinction of two intervals with higher values of susceptibility: the top of GA3 and GA4 profiles and the bottom of GA1 and GA2 profiles.

In the absence of other proxies for a detailed lateral correlation among the profiles, the low susceptibility values of GA1 are correlated with GA2 and GA3 with GA4 profiles, allowing to clarify the relation between the NW and NE walls. We decide to consider the profiles in NW wall, GA2 and GA4, as references for this correlation since they reach greater depth. In order to better understand the concentration of magnetic minerals present in the samples, we extend the correlation previously proposed to that including the isothermal remanent magnetization measured at 1T (IRM_{1T}) and HIRM, defined by 0.5 ×(IRM_{1T} + $IRM_{0.33T}$), which provides the ferrimagnetic material contribution and the high coercivity fraction (hematite and goethite), respectively. The low field susceptibility (Figures **7** and 8a) evidences a major concentration of magnetic minerals at the bottom part of the profiles; in detail, GA1 presents higher values than GA2. On the contrary, the IRM_{1T} (Figure 8b) parameter suggests a higher concentration of the high coercivity minerals for GA2 than GA1, especially in the upper part of the profiles. The presence of high coercivity minerals is later confirmed by the HIRM profile (Figure 8b,c). The results suggest that the susceptibility trend at the bottom of GA1 is caused by changes in the content of ferrimagnetic and high coercivity minerals, while at the upper part of GA2, the susceptibility profile mimics the HIRM distribution. However, similar tendencies at a different depth and amplitude indicate a different sedimentation rate, perhaps due to intensity variations of floods and/or their altering frequency, as suggested by other authors focusing on cave sediments [3].

GA3 and GA4 profiles are characterized by a larger amplitude in the variation of their magnetic properties in the ferromagnetic fraction (Figure 9a), total magnetic contribution (Figure 9b), and high coercivity minerals (Figure 9c) particularly in the top section.

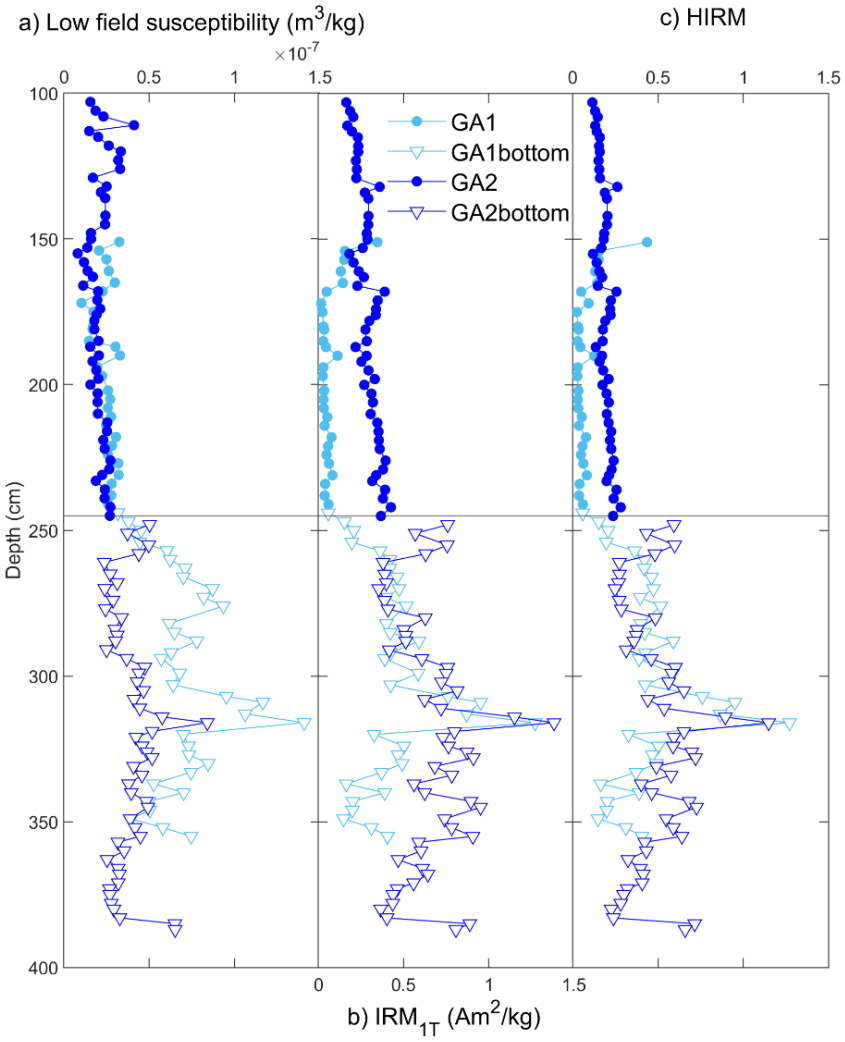

Figure 8. Magnetic parameters at GA1 and GA2 profiles with depth. (**a**) Low magnetic field susceptibility; (**b**) IRM_{1T} and (**c**) HIRM, defined as (IRM_{1T} + $IRM_{0.33T}$)/2.

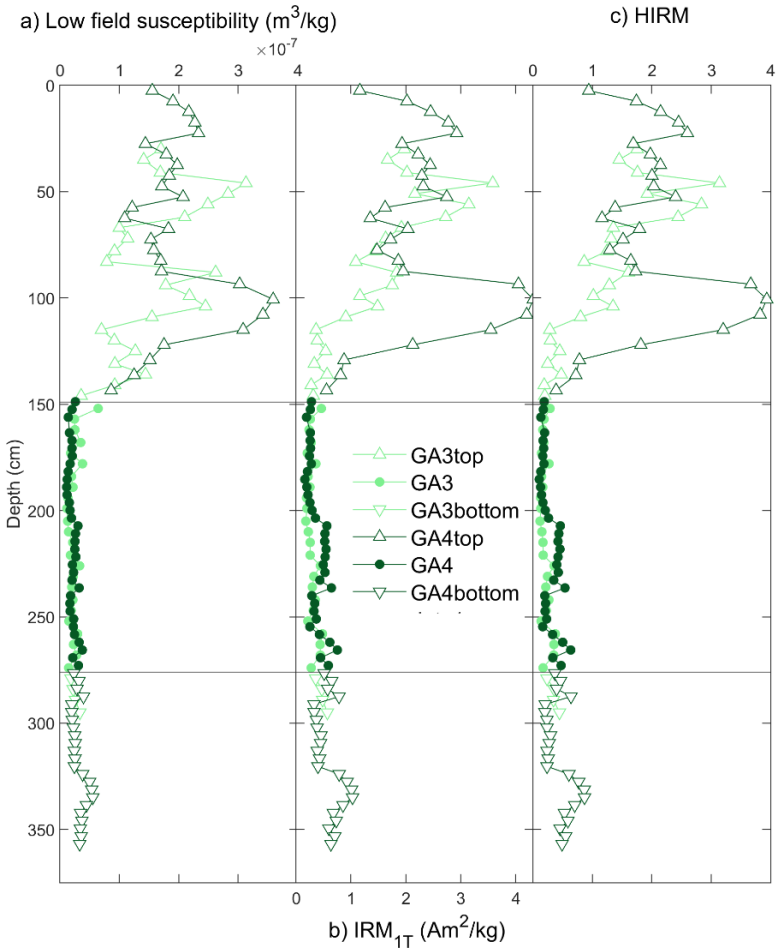

Figure 9. Magnetic parameters of GA3 and GA4 with depth. (**a**) Low magnetic field susceptibility; (**b**) IRM_{1T} and (**c**) HIRM, defined as $(IRM_{1T} + IRM_{0.33T})/2$.

In order to discriminate the relative concentration of each magnetic component in GA1 and GA2 profiles, the relative contribution of magnetite versus goethite and hematite, M/GH (Figure 10a), is illustrated, and goethite versus hematite, G/H (Figure 10b). GA1 is characterized by three different intervals. The bottom part where the M/GH demonstrates that the higher susceptibility is provided by abundant magnetite at GA1 than GA2. In the upper part, another two intervals with a different magnetite contribution are identified: one until around 180 cm depth and a final increase of magnetite upward. These variations of magnetite on the upper part were not identified on the susceptibility record, probably covered by the significant presence of high coercivity minerals (Figure 7).

4.3 Magnetic Grain Size Analysis

Figure 11 shows the results of magnetic grain size analysis from sections GA1 and GA2 where it has been evidenced the position of the samples from the top and bottom part of the section. All the samples considered fall in the Pseudo-Single Domain (PSD) field although those of the bottom section are distributed near the SD-MD mixing curve and the other samples are located at the middle of the PSD area, indicating a higher SP-SD concentration (from the guide curve proposed by reference [51]). This observation can also suggest a higher contribution of maghemite [58].

A further plot to analyse the magnetic grain size, based on the relationship between anhysteretic and low field susceptibilities, is the King plot [52]. It presents steeper slopes for smaller grains. Figure 12 summarizes the results of the four profiles subdivided into the three sections identified. Data can be grouped into three different grain size categories: the smaller fraction is mainly composed of the bottom section samples and some samples of GA3 and GA4 profiles; the highest grain size is composed of the middle section samples. Finally, the samples from the middle section present a mid-grain size.

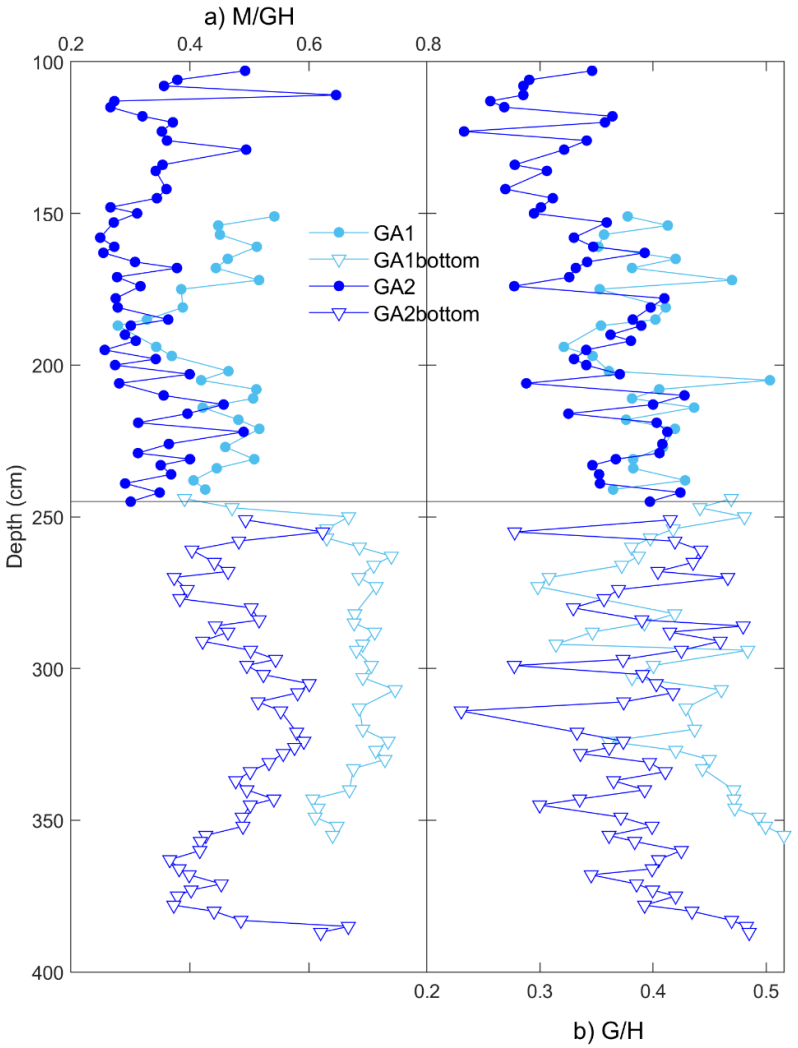

Figure 10. Magnetic mineral discrimination of GA1 and GA2, in detail: (**a**) Concentration of magnetite versus goethite and hematite; (**b**) Concentration of goethite versus hematite.

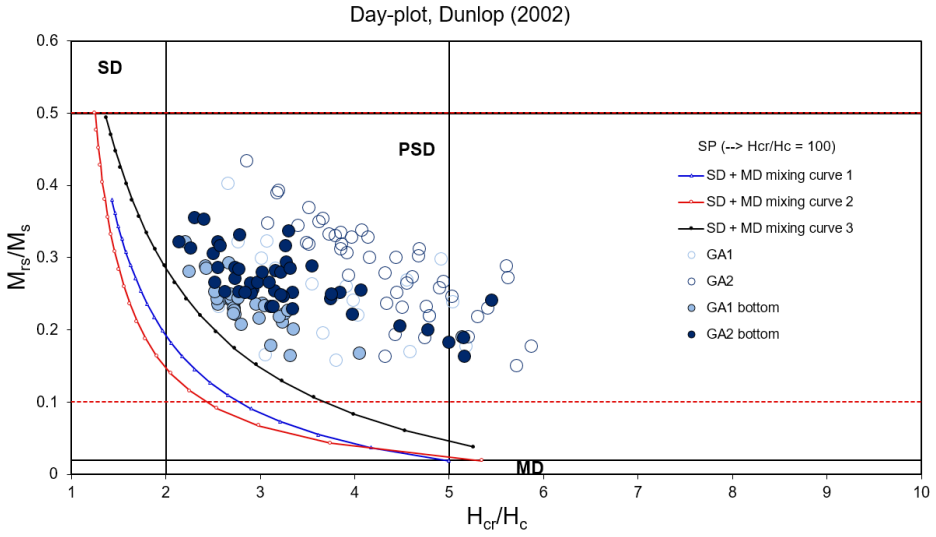

Figure 11. Day-plot diagram for samples from GA1 and GA2. Open symbols correspond to the top part of the sections and full symbols to the bottom part as defined in Figure 7.

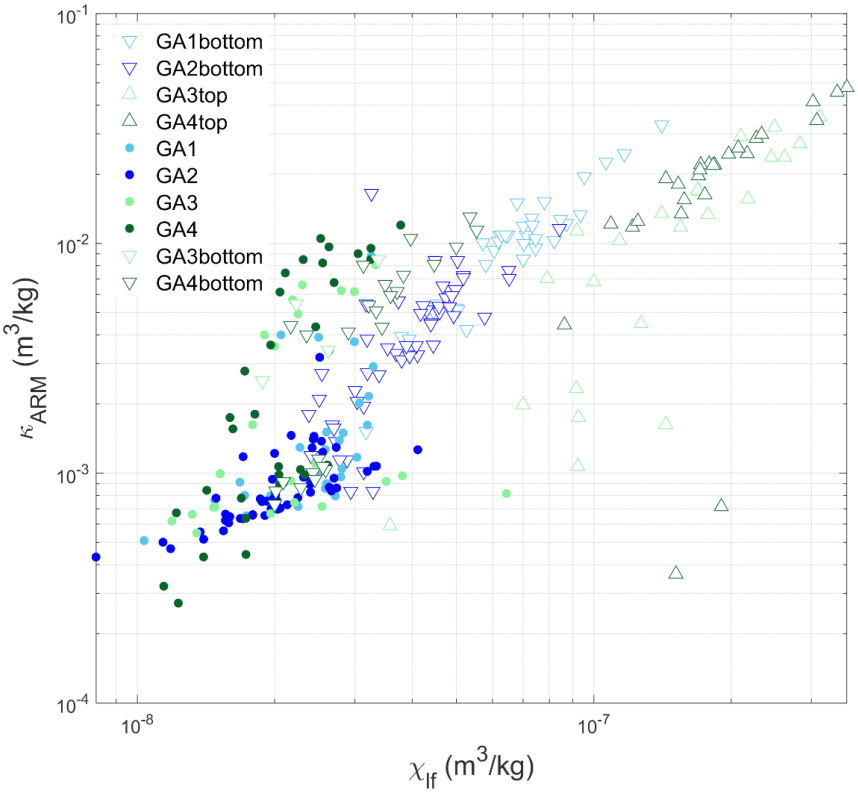

Figure 12. King plot of all the profiles considered in the study with a distinction of the top of GA3 and GA4 and bottom of GA1 and GA2. The bottom section of all four profiles shows a small grain size, the middle section larger particles and the top section a mid-size particles.

A closer look into the magnetic grain size distribution in relation to the depth is presented in Figure 13 with the IRM_{1T}/χ_{lf} ratio with respect to depth. This ratio varies inversely with magnetic grain size, could be influenced by the presence of high coercivity minerals, and is particularly sensitive to higher grain particles (>10 μm [48]).

The magnetic grain size does not present significant variations on the GA2 profile (Figure 13a), except on the upper part where lower values propose an increase of grain size. The GA1 profile shows a higher grain size at the upper part. Through GA3 and GA4 profiles (Figure 13b), the ratio reveals a progressive increase of grain size upward and a slight decrease at the top. The lower values of the ratio on the GA3 profile reflect a higher grain size than GA4. The variation of grain size at the lower part of the profiles was not evidenced on the other concentration parameters, while the trend at the top corresponds with higher contributions of ferrimagnetic and canted antiferromagnetic minerals.

Elemental geochemistry is usually used to detect post-depositional dissolution of magnetic minerals that affect the magnitude of magnetic properties [59]. Figure 14 shows the percentage of *S*, *P* and *Fe* compared to the corresponding low field susceptibility from profiles GA1 and GA3 (raw data of elemental geochemistry is shown in Table S1). A relevant concentration of S (Figure 14a) at the top shows a good correlation with higher values of low field susceptibility at the top of the GA3 profile (Figure 14d), coincident with lowest values of P (Figure 14b) and a relative increase of Fe (Figure 14c). The presence of sulphur may be found in the degradation of bat guano, coming from the upper GII unit. In fact, among the minerals produced by the fungal degradation of bat guano, we found crandallite as a result of the interaction between a slightly acidic phosphate solution and Ca-Al sediments [60]. The presence of crandallite was documented in GIa [15] and GIb [10].

The Fe trend shows a good correlation with the low field susceptibility at the top and middle profile, while at the bottom a slight decrease of Fe corresponds with the enhanced susceptibility of the GA1 profile (Figure 14c,e).

The presence of phosphorus was already detected in previous studies and attributed to the leaching from the GII unit [15]. A delimited interval with high values of P near the boundary with the top section could be due to different sedimentological characteristics of this part that delay the leaching process.

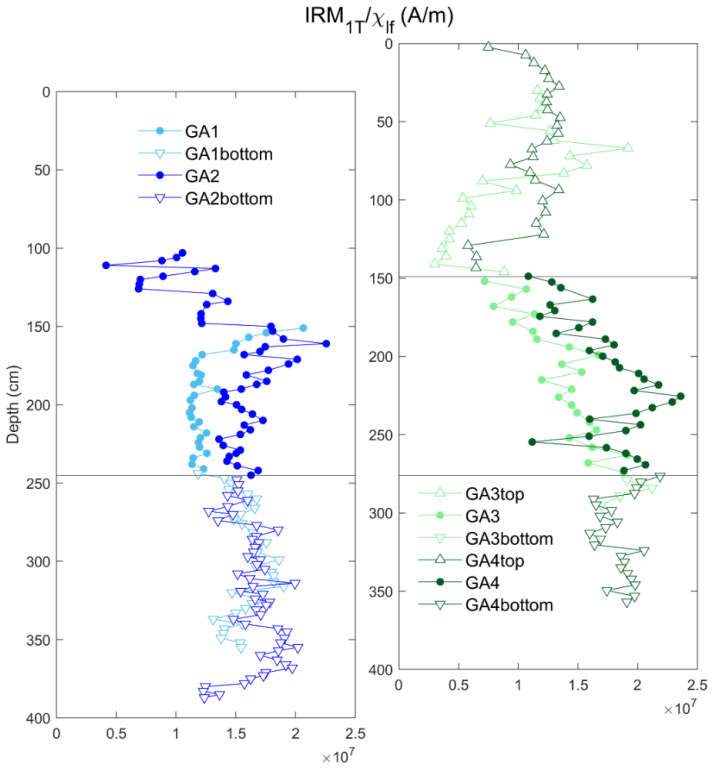

Figure 13. Magnetic grain size analysis with ratio IRM_{1T}/χ_{lf} with respect to the depth: (**a**) GA1 and GA2; (**b**) GA3 and GA4.

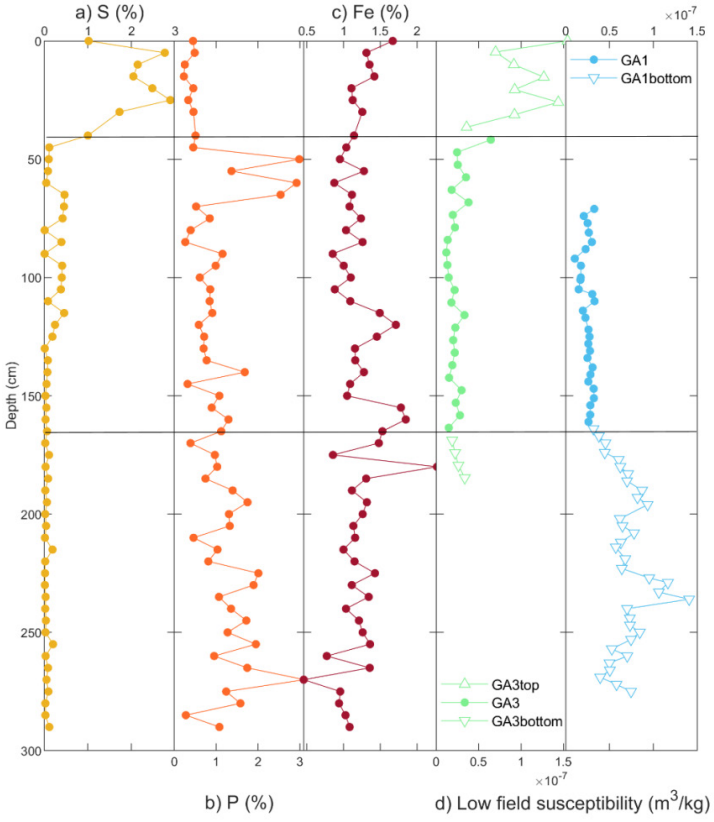

Figure 14. Plots of: (**a**) S; (**b**) P; (**c**) Fe in % with depth and in comparison with (**d**) low field susceptibility of GA3 and GA1.

Some elemental ratios have been used to emphasise the different mobility of elements preferentially hosted in different minerals [53]: Rb usually is concentrated in phyllosilicates and K-feldspar, Sr could be found in plagioclase in most weathering conditions (more easily removed during the weathering; [61–63]) and Fe, mainly contained on the Fe oxide minerals, is relatively mobile under common post-depositional conditions [3]. Figure 15 shows the ratios Sr/Ba, Rb/Sr and Ti/Fe with the low magnetic field susceptibility of GA3 and GA1 profiles. These ratios evidence a higher weathering degree at the top of GA3, related with higher values of the low field susceptibility, and at the bottom of GA1; a similar situation was described and interpreted by references [53,64]. Moreover, the Ti/Fe ratio, a proxy of the presence of iron oxides (strictly magnetite and hematite, [65]), provides a good correlation with low field susceptibility variations at the bottom, a weak enhancement in the middle and a decrease at the top section. A decrease of this ratio may indicate an increase of erosion in the source area.

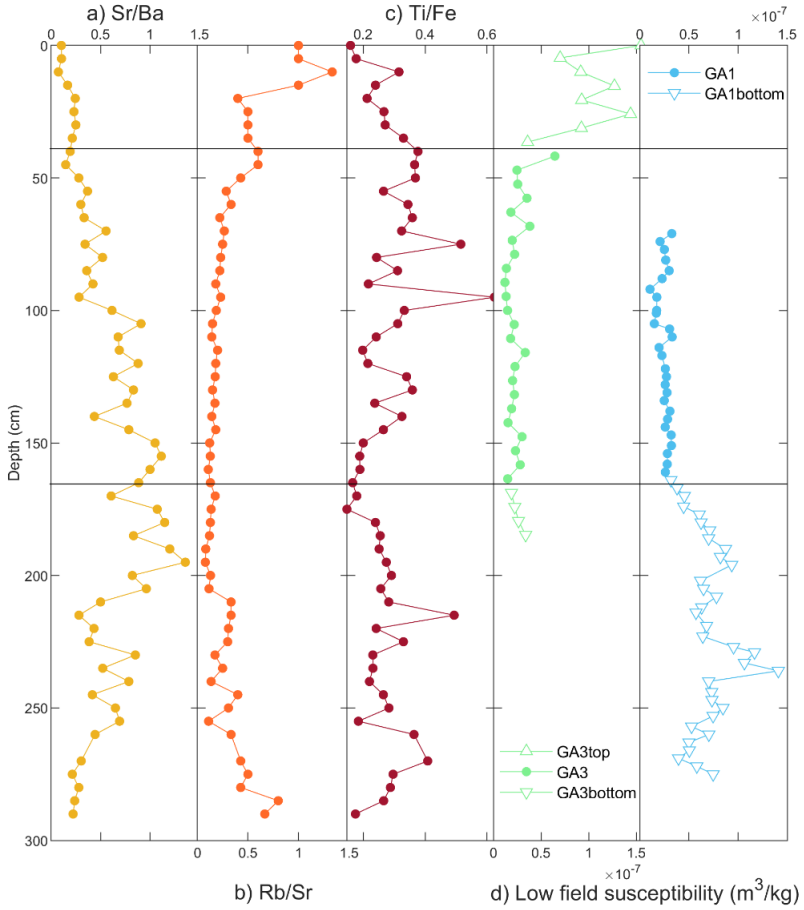

Figure 15. Plots of: (**a**) Sr/Ba; (**b**) Rb/Sr; (**c**) Ti/Fe with depth and in comparison with (**d**) Low field susceptibility of GA3 and GA1 profiles.

5. Discussion

The overall stratigraphic record analysed in the cave of Covacha de los Zarpazos includes a GI unit, made of waterlain deposits. Despite a complete sedimentary reconstruction of this unit that was recently presented by reference [15], this work provides the first rockmagnetic analysis of these sediments. Three different aspects have been taken into account for the environmental reconstruction: the pedogenic processes, the water-flow activity and geochemical indicators of weathering.

For the magnetic mineral assemblages and their climate interpretation, a previous environmental reconstruction of the GI unit from the Galería site [5] suggests a humid environment, with increased precipitation and decreasing vegetation cover for the GIa subunit. This conclusion is based on the coarser composition of sand with evidences of surface erosion and fine-grained goethite. GIb subunit, on the contrary, presents a reduced presence of magnetite and high goethite concentration, close-cave conditions, a thin and discontinuous bat guano horizon and an alternation of humid and dry

periods, as suggested by the fluctuations of goethite presence. Also, hematite presence was documented in all Galería samples.

In our study, the main magnetic minerals present have been found to be magnetite (dominant), traces of maghemite, hematite and goethite (Figure 4). This identification is supported by hysteresis loops in sample GA1-42 showing the presence of a larger contribution of high coercivity minerals than GA1-50 (Figure 3a,b). In detail, all samples show the presence of hematite in the thermomagnetic curves (Figure 4), which is identified by the disappearance of susceptibility at 700 ºC. Goethite is identified by a slight decrease of the heating curve at the temperature range of 100–120 ºC (Figure 4d), although its hidden presence on the other samples could be due to the high crystallinity size/degree. Furthermore, the cooling curves lower than heating (Figure 4a,b) could indicate a partial oxidation of magnetite to maghemite that after heating is oxidised to hematite in samples from GA1 profile [66]. The difference in progressive acquisition curves of IRM (Figure 5) suggests variations in the contribution of magnetite and hematite/goethite. The coercivity analysis (Figure 6) infers a dominant presence of magnetite in the lower part of GA1 and GA2 profiles and a major concentration of high coercivity minerals upward.

We distinguish three different sections on the entire sedimentary sequence analysed, namely the bottom, middle and top section. The bottom part is characterized by a low variability of the low field susceptibility in the four analysed profiles (Figure 7). Low field susceptibility correlates well with IRM at 1T suggesting the dominance of ferromagnetic phases (magnetite/maghemite) to the overall contribution of the sediments (Figures 8 and 9), associated with warm and temperate climatic conditions in soils [67] and intervals not significantly pedogenic altered [68]. Moreover, although the G/H ratio (Figure 10b) presents weak variations, suggesting a relatively constant redox condition along the profiles, a slightly higher contribution of goethite is identified at the bottom section, particularly in the GA1 profile. The predominance of goethite versus hematite indicates higher humid conditions, as well as apparent climatic deterioration at the deposition time [3]. The higher goethite concentration could be due to: the low intensity of pedogenic processes, inhibiting climatic conditions for hematite formation (e.g., more acidic environments [69,70]); local reducing environment responsible for the reduction of hematite to magnetite [71]; a secondary formation of goethite caused by the hydration of hematite [72].

Higher up in the sequence, the middle part presents a slightly lower value of the low field susceptibility (Figure 7), accompanied by the decrease of magnetic minerals concentration (Figures 8 and 9), which may suggest a cold interval inhibiting the formation and/or deposition of magnetite [67]. The increased hematite concentration at this middle section may suggest ventilated areas [70] and confirm colder conditions. These characteristics could represent the preparation phase of the cave for the imminent opening to the outside.

The other factor to consider in the cave analysed is the water activity since the interior of the GI unit was individuated in the passage from epi-phreatic to vadose conditions [15]. Generally, reducing conditions are suggested by the presence of Fe^{2+} just below the vadose-phreatic boundary [73] and seasonal fluctuations of water table levels usually promote the cyclic dissolution of both ferrous and ferric minerals [74]. Also, the magnetic minerals could indicate a particular hydrodynamic condition. The predominance of hematite usually indicates environments with low water activity [75], as observed in the middle section.

A previous study on Galería Complex [19] analyses the anisotropy of magnetic susceptibility in order to reconstruct the underground water activity. They observe a slightly higher anisotropy value for GI unit, suggesting a relatively higher hydrodynamic regime with respect to the GIII unit.

In the absence of anisotropy measurements here, grain size analysis might provide information about the water flux intensity (Figure 12). The smaller magnetic grain size observed on the bottom section could be due to less intensive floods as proposed by reference [3]. The mid magnetic grain size is shown on the top section and the lower grain size on the middle section.

Finally, the elemental geochemistry analysis provides information about the weathering processes suffered by sediments. The elemental ratios analysed in this study suggest a higher weathering degree on the bottom and on the top of our profiles. Also, the presence of high coercivity minerals (hematite and goethite) could indicate oxidative weathering and soil-forming processes [76]. Among the weathering processes of this facies was identified the acidic leaching of the bat guano deposit of the GII unit, forming phosphates like crandallite, $CaAl_3(PO_4)_2(OH)_5{\cdot}H_2O$ present in nodules in most layers of GIa [10,14,15]. The infiltration of these phosphate solutions through the cave sediments depends on moisture (influenced by local climate and cave types) and lithology/porosity of the sedimentary sequence.

The weathering development could correlate also

with the magnetic grain size since the high coercivity of less weathering samples could be caused by low-temperature oxidation of the coarsed-grained (PSD and MD) magnetic particles whereas the low coercivity of magnetic minerals could indicate newly pedogenic products and probably they located just above the SP/SD boundary resulting completely oxidated into maghemite [17]. The middle section is mainly composed of high coercivity minerals arranged near the SP/SD curve (Figure 11), confirming the oxidation to maghemite (observed in Figure 4). The low field susceptibility seems to be also correlated to the Sr/Ba and Rb/Sr ratios, suggesting a significant degree of weathering (Figure 15).

The top part of the section is only represented by GA3 and GA4 and shows the highest values of susceptibility probably due to a local reducing environment for the higher presence of organic matter [77]. These conditions allow the hematite to be reduced to magnetite [71] and subsequently oxidized into maghemite. The higher weathering degree of this section, evidenced by Sr/Ba and Rb/Sr, suggests higher pedogenesis intensity [18] and warmer intervals. Finally, the top section represents probably the final deposition step before the ceiling collapse, in which the decrease of Ti/Fe ratio (Figure 15) indicates local erosional processes and the presence of sulphur documented in arid conditions [78,79].

6. Conclusions

The analysis of magnetic properties and elemental geochemistry applied to waterlain facies of the Covacha de los Zarpazos cave sediments provides features of the depositional environment and post-depositional processes:

- The presence of different magnetic minerals is identified: low coercivity minerals (magnetite and trace of maghemite) and high coercivity minerals (hematite and goethite).
- NE and NW walls of the cave are correlated for the first time by means of low field susceptibility values.
- Three different sections are identified into the GI unit, provide a more detailed environmental reconstruction than stratigraphic and sedimentological approach.
- Warm, template and humid conditions are suggested for the bottom section, with no significantly intense pedogenesis process.
- The middle section shows colder conditions and ventilated areas.
- Finally, the top section presents a reducing environment and warmer conditions.

This study thus shed light on the correlation of the magnetic signals with the development of climatic conditions, the hydrological changes of the groundwater river responsible for the deposition of the waterlain facies and post-depositional weathering processes. Further analysis aimed at quantifying each magnetic mineral could provide more details on the environmental changes, and accurate dating analysis of these sediments could provide precious information on the Quaternary climate fluctuations.

Author Contributions

Conceptualization, methodology, software, S.D., J.M.P., F.M.H.; validation, J.M.P. and F.M.H.; formal analysis, investigation, S.D.; resources, data curation, J.M.P. and F.M.H.; writing-original draft preparation, S.D.; writing-review and editing, S.D., J.M.P., F.M.H.; visualization, supervision, J.M.P. and F.M.H.; project administration, funding acquisition, J.M.P. All authors have read and agreed to the published version of the manuscript.

Conflict of Interest

The authors disclosed no conflict of interest.

Data Availability Statement

The data used on this study are the measures of magnetic properties of some samples take from the archaeological sites. So, the data are not available to access.

Funding

This research received funding by Grant PID2021-122355NB-C33 funded by MCIN/AEI/10.13039/ 5011 00011033/FEDER, UE.

Acknowledgments

The authors want to thank the Proyecto Atapuerca, Fundación Atapuerca and the Junta de Castilla y León for continuous support to the research in the Atapuerca archaeological sites. A personal acknowledgment to the researcher Nicolás González Santacruz for the contribution on the analysis of GA3 and GA4 profiles. This work has benefited from discussion with all the researchers with experience on this cave. This work is partially sponsored by Grant PID2021-122355NB-C33 funded by MCIN/AEI/10.13039/501100011033/FEDER, UE; MICINN-PID2021-122355NB-C32, the 2021 SGR 01238 (AGAUR), the 2023PFR-URV-01238 (URV) projects and "María de Maeztu" excellence accreditation (CEX2019-000945-M). A particular acknowledg-

ment for the reviewers as well as the editors for their constructive and helpful comments that led to the improvement of this article.

Supplementary Materials

The supporting information can be downloaded at: https://journals.nasspublishing.com/files/EPS-1108-Supplementary-Materials.pdf

References

[1] D'Arcangelo, S., Martín-Hernández, F., Parés, J.M., 2021. Magnetic properties of cave sediments at Gran Dolina site in Sierra de Atapuerca (Burgos, Spain). Quaternary International. 583, 1–13. DOI: https://doi.org/10.1016/j.quaint.2021.02.041

[2] D'Arcangelo, S., Martín-Hernández, F., Parés, J.M., 2023. Environmental reconstruction from the identification of magnetic minerals in the upper sedimentary infill of the Gran Dolina cave (Burgos, Spain). Applied Sciences. 13(7), 4580. DOI: https://doi.org/10.3390/app13074580

[3] Šroubek, P., Diehl, J.F., Kadlec, J., 2007. Historical climatic record from flood sediments deposited in the interior of Spirálka Cave, Czech Republic. Palaeogeography, Palaeoclimatology, Palaeoecology. 251(3–4), 547–562. DOI: https://doi.org/10.1016/j.palaeo.2007.05.001

[4] Aidona, E., Pechlivanidou, S., Pennos, C., 2017. Environmental magnetism: Application to cave sediments. Bulletin of the Geological Society of Greece. 47(2), 892. DOI: https://doi.org/10.12681/bgsg.11128

[5] Bógalo, M.F., Bradák, B., Villalaín, J.J., et al., 2021. High-resolution late Middle Pleistocene paleoclimatic record from the Galería Complex, Atapuerca archaeological site, Spain—An environmental magnetic approach. Quaternary Science Reviews. 251, 106721. DOI: https://doi.org/10.1016/j.quascirev.2020.106721

[6] Goldberg, P., Sherwood, S.C., 2006. Deciphering human prehistory through the geoarcheological study of cave sediments. Evolutionary Anthropology: Issues, News, and Reviews. 15(1), 20–36. DOI: https://doi.org/10.1002/evan.20094

[7] Karkanas, P., Goldberg, P., 2019. Reconstructing Archaeological Sites: Understanding the Geoarchaeological Matrix, 1st ed. Wiley-Blackwell: UK. DOI: https://doi.org/10.1002/9781119016427

[8] Arnold, L.J., Demuro, M., Parés, J.M., et al., 2015. Evaluating the suitability of extended-range luminescence dating techniques over early and Middle Pleistocene timescales: Published datasets and case studies from Atapuerca, Spain. Quaternary International. 389, 167–190. DOI: https://doi.org/10.1016/j.quaint.2014.08.010

[9] Berger, G.W., Pérez-González, A., Carbonell, E., et al., 2008. Luminescence chronology of cave sediments at the Atapuerca paleoanthropological site, Spain. Journal of Human Evolution. 55(2), 300–311. DOI: https://doi.org/10.1016/j.jhevol.2008.02.012

[10] Demuro, M., Arnold, L.J., Parés, J.M., et al., 2014. New Luminescence Ages for the Galería Complex Archaeological Site: Resolving Chronological Uncertainties on the Acheulean Record of the Sierra de Atapuerca, Northern Spain. PLoS ONE. 9(10), e110169. DOI: https://doi.org/10.1371/journal.pone.0110169

[11] Falguères, C., Bahain, J.J., Yokoyama, Y., et al., 2001. Datation par RPE et U-Th des sites pléistocènes d'Atapuerca: Sima de los Huesos, Trinchera Dolina et aTrinchera Galería. Bilan géochronologique. L'Anthropologie. 105(1), 71–81. DOI: https://doi.org/10.1016/S0003-5521(01)80006-6

[12] Falguères, C., Bahain, J.J., Bischoff, J.L., et al., 2013. Combined ESR/U-series chronology of Acheulian hominid-bearing layers at Trinchera Galería site, Atapuerca, Spain. Journal of Human Evolution. 65(2), 168–184. DOI: https://doi.org/10.1016/j.jhevol.2013.05.005

[13] Grün, R., Aguirre, E. 1987. Datación por ESR y por la serie del U, en los depósitos cársticos de Atapuerca. In: Aguirre, E., Carbonell, E., Castro, J.M.B. (eds). El Hombre Fósil de Ibeas y el Pleistoceno de la Sierra de Atapuerca: I. Junta de Castilla y León: Valladolid. pp. 201–204.

[14] Pérez-González, A., Parés, J.M., Gallardo, J., et al., 1999. Geología y estratigrafía del relleno de Galería de la Sierra de Atapuerca (Burgos) en: Carbone-11, E. In: Roura, E.C., González, A.R., Fernández-Lomana, J.C.D. (eds). Atapuerca: Ocupaciones Humanas y Paleoecología del Yacimiento de Galería. Junta de Castilla y León: Valladolid. pp. 31–42.

[15] Campaña, I., Benito-Calvo, A., Pérez-González, A., et al., 2023. Reconstructing depositional environments through cave interior facies: The case of Galería Complex (Sierra de Atapuerca, Spain). Geomorphology. 440, 108864. DOI: https://doi.org/10.1016/j.geomorph.2023.108864

[16] Jordanova, D., Grygar, T., Jordanova, N., et al., 2006. Palaeoclimatic significance of hematite/goethite ratio in Bugarian loess-paleosol sediments deduced by DRS and rock magnetic measurements. In: Petrovský, E., Ivers, D., Harinarayana, T., et al. (eds). The Earth's Magnetic Interior. Springer: Dordrecht. pp. 399–412.
DOI: https://doi.org/10.1007/978-94-007-0323-0_26

[17] Liu, Q., Torrent, J., Maher, B.A., et al., 2005. Quantifying grain size distribution of pedogenic magnetic particles in Chinese loess and its significance for pedogenesis. Journal of Geophysical Research: Solid Earth. 110(B11), B11102.
DOI: https://doi.org/10.1029/2005JB003726

[18] Bloemendal, J., Liu, X., Sun, Y., et al., 2008. An assessment of magnetic and geochemical indicators of weathering and pedogenesis at two contrasting sites on the Chinese Loess plateau. Palaeogeography, Palaeoclimatology, Palaeoecology. 257(1–2), 152–168.
DOI: https://doi.org/10.1016/j.palaeo.2007.09.017

[19] Parés, J.M., Pérez-González, A., Arsuaga, J.L., et al., 2010. Characterizing the sedimentary history of cave deposits, using Archaeomagnetism and rock magnetism, Atapuerca (Northern Spain). Archaeometry. 52(5), 882–898.
DOI: https://doi.org/10.1111/j.1475-4754.2010.00533.x

[20] Ortega, A.I., 2009. La evolución geomorfológica del karst de la Sierra de Atapuerca (Burgos) y su relación con los yacimientos Pleistocenos que contiene [PhD thesis]. Burgos: Universidad de Burgos. p. 200.
DOI: https://doi.org/10.36443/10259/7143

[21] Ortega, A.I., Benito-Calvo, A., Pérez-González, A., et al., 2013. Evolution of multilevel caves in the Sierra de Atapuerca (Burgos, Spain) and its relation to human occupation. Geomorphology. 196, 122–137.
DOI: https://doi.org/10.1016/j.geomorph.2012.05.031

[22] Pérez-González, A., Aleixandre, T., Pinilla, A., et al., 1995. An approach to the Galería stratigraphy in the Sierra de Atapuerca trench (Burgos). In: de Castro, J.M.B., Carbonell, E., Arsuaga, J.L. (eds). Human Evolution in Europe and the Atapuerca Evidence. Junta de Castilla y León: Valladolid. pp. 99–122.

[23] Pérez-González, A., Parés, J.M., Carbonell, E., et al., 2001. Géologie de la Sierra de Atapuerca et stratigraphie des remplissages karstiques de Galería et Dolina (Burgos, Espagne). L'Anthropologie. 105(1), 27–43.
DOI: https://doi.org/10.1016/S0003-5521(01)80004-2

[24] Bermejo, L., Ortega, A.I., Guérin, R., et al., 2017. 2D and 3D ERT imaging for identifying karst morphologies in the archaeological sites of Gran Dolina and Galería Complex (Sierra de Atapuerca, Burgos, Spain). Quaternary International. 433, 393–401.
DOI: https://doi.org/10.1016/j.quaint.2015.12.031

[25] Parés, J.M., Álvarez, C., Sier, M., et al., 2018. Chronology of the cave interior sediments at Gran Dolina archaeological site, Atapuerca (Spain). Quaternary Science Reviews. 186, 1–16.
DOI: https://doi.org/10.1016/j.quascirev.2018.02.004

[26] Campaña, I., Benito-Calvo, A., Pérez-González, A., et al., 2022. Revision of TD1 and TD2 stratigraphic sequence of Gran Dolina cave (Sierra de Atapuerca, Spain). Journal of Iberian Geology. 48(4), 425–443.
DOI: https://doi.org/10.1007/s41513-022-00200-8

[27] Ortega, A.I., Benito, A., Pérez-González, A., et al., 2014. Atapuerca karst and its palaeoanthropological sites. In: Gutiérrez, F., Gutiérrez, M. (eds). Landscapes and Landforms of Spain. Springer: Dordrecht. pp. 101–110.
DOI: https://doi.org/10.1007/978-94-017-8628-7_8

[28] Cáceres, I., 2002. Tafonomia de yacimientos antrópicos en karst. Complejo Galería (Sierra de Atapuerca, Burgos), Vanguard Cave (Gibraltar) y Abric Romaní (Capellades, Barcelona) [PhD thesis]. Tarragona: Universitat Rovira i Virgili. p. 100.

[29] Ollé, A., Cáceres, I., Vergès, J.M., 2005. Human occupations at Galería site (Sierra de Atapuerca, Burgos, Spain) after the technological and taphonomical data. In: Molines, N., Moncel, M.H., Monnier, J.L. (eds). Les Premiers Peuplements en Europe. Colloque International: Données Récentes sur les Modalités de Peuplement et sur le Cadre Chronostratigraphique, Géologique et Paléogéographique des Industries du Paléolithique Ancien et Moyen en Europe (Rennes, 22–25 Septembre 2003). John and Erika Hedges Ltd: Oxford. pp. 269–280.

[30] Cáceres, I., Huguet, R., Rosell, J., et al., 2010. El yacimiento de Galería (Sierra de Atapuerca, Burgos, España): un enclave para la obtención de recursos cárnicos en el Pleistoceno Medio. Zona arqueológica. 13, 186–196.

[31] García-Medrano, P., Cáceres, I., Ollé, A., et al., 2017. The occupational pattern of the Galería site (Ata-

puerca, Spain): A technological perspective. Quaternary International. 433, 363–378.
DOI: https://doi.org/10.1016/j.quaint.2015.11.013

[32] Bermúdez de Castro, J.M., Rosas, A., 1992. A human mandibular fragment from the Atapuerca Trench (Burgos, Spain). Journal of Human Evolution. 22(1), 41–46.
DOI: https://doi.org/10.1016/0047-2484(92)90028-8

[33] Head, M.J., Pillans, B., Farquhar, S.A., 2008. The Early—Middle Pleistocene Transition: characterization and proposed guide for the defining boundary. Episodes. 31(2), 255–259.
DOI: https://doi.org/10.18814/epiiugs/2008/v31i2/014

[34] Head, M.J., Gibbard, P.L., 2015. Early–Middle Pleistocene transitions: Linking terrestrial and marine realms. Quaternary International. 389, 7–46.
DOI: https://doi.org/10.1016/j.quaint.2015.09.042

[35] Ollé, A., Huguet, R., 1999. Secuencia arqueoestratigráfica del yacimiento de Galería, Atapuerca. In: Roura, E.C., González, A.R., Fernández-Lomana, J.C.D. (eds). Atapuerca: Ocupaciones humanas y paleoecología del yacimiento de Galería. Junta de Castilla y León: Valladolid. pp. 55–62.

[36] Vallverdú, P., 1999. Microfacies y micromorfología de GII y GIII de Trinchera Galería. In: Roura, E.C., González, A.R., Fernández-Lomana, J.C.D. (eds). Atapuerca: Ocupaciones humanas y paleoecología del yacimiento de Galería. Junta de Castilla y León: Valladolid. pp. 43–55.

[37] Galindo-Pellicena, M.A., Cuenca-Bescós, G., Arsuaga, J.L., 2011. Los micromamíferos (Rodentia, Soricomorpha, Erinaceomorfa, Lagomorpha y Chiroptera) del Pleistoceno Medio de la Covacha de los Zarpazos (Sierra de Atapuerca, Burgos, España). Boletín de la Real Sociedad Española de Historia Natural. Sección Geológica. 105(1–4), 87–97.

[38] Rosas, A., Bermúdez de Castro, J.M., 1999. Descripción y posición evolutiva de la mandíbula AT76-T1H del yacimiento de Galería (Sierra de Atapuerca). In: Roura, E.C., González, A.R., Fernández-Lomana, J.C.D. (eds). Atapuerca: Ocupaciones Humanas y Paleoecología del Yacimiento de Galería. Consejería de Educación y Cultura: Valladolid. pp. 237–244.

[39] Arsuaga, J.L., Gracia, A., Lorenzo, C., et al., 1999. Resto craneal humano de Galería/Cueva de los Zarpazos (Sierra de Atapuerca). In: Roura, E.C., González, A.R., Fernández-Lomana, J.C.D. (eds). Atapuerca: Ocupaciones Humanas y Paleoecología del Yacimiento de Galería. Consejería de Educación y Cultura: Valladolid. pp. 233–236.

[40] Rosas, A., Carbonell, E., Ollé, A., et al., 1999. Contribución del yacimiento de Galería (Sierra de Atapuerca) al Cuaternario Ibérico. In: Roura, E.C., González, A.R., Fernández-Lomana, J.C.D. (eds). Atapuerca: Ocupaciones Humanas y Paleoecología del Yacimiento de Galería. Consejería de Educación y Cultura: Valladolid. pp. 377–390.

[41] Néel, L., 1949. Théorie du traînage magnétique des ferromagnétiques en grains fins avec applications aux terres cuites. Annales de Géophysique 5, 99–136.

[42] Egli, R., 2009. Magnetic susceptibility measurements as a function of temperature and frequency I: inversion theory. Geophysical Journal International. 177(2), 395–420.
DOI: https://doi.org/10.1111/j.1365-246X.2009.04081.x

[43] Dearing, J.A., Dann, R.J.L., Hay, K., et al., 1996. Frequency-dependent susceptibility measurements of environmental materials. Geophysical Journal International. 124(1), 228–240.
DOI: https://doi.org/10.1111/j.1365-246X.1996.tb06366.x

[44] Stober, J.C., Thompson, R., 1979. Magnetic remanence acquisition in Finnish lake sediments. Geophysical Journal International. 57(3), 727–739.
DOI: https://doi.org/10.1111/j.1365-246X.1979.tb06786.x

[45] Liu, Q., Roberts, A.P., Torrent, J., et al., 2007. What do the HIRM and S-ratio really measure in environmental magnetism? Geochemistry, Geophysics, Geosystems. 8, Q09011.
DOI: https://doi.org/10.1029/2007GC001717

[46] Kruiver, P.P., Dekkers, M.J., Heslop, D., 2001. Quantification of magnetic coercivity components by the analysis of acquisition curves of isothermal remanent magnetization. Earth and Planetary Science Letters. 189(3–4), 269–276.
DOI: https://doi.org/10.1016/S0012-821X(01)00367-3

[47] Egli, R., 2003. Analysis of the field dependence of remanent magnetization curves. Journal of Geophysical Research: Solid Earth. 108(B2), 2081.
DOI: https://doi.org/10.1029/2002JB002023

[48] Roberts, A.P., Reynolds, R.L., Verosub, K.L., et al., 1996. Environmental magnetic implications of Greigite (Fe_3S_4) Formation in a 3 m.y. lake sediment record from Butte Valley, northern Califor-

nia. Geophysical Research Letters. 23(20), 2859–2862.
DOI: https://doi.org/10.1029/96gl02831

[49] Kodama, K.P., Hinnov, L.A., 2014. Rock Magnetic Cyclostratigraphy, 1st ed. John Wiley & Sons: USA.
DOI: https://doi.org/10.1002/9781118561294.ch2

[50] Day, R., Fuller, M., Schmidt, V.A., 1977. Hysteresis properties of titanomagnetites: Grain-size and compositional dependence. Physics of the Earth and Planetary Interiors. 13(4), 260–267.
DOI: https://doi.org/10.1016/0031-9201(77)90108-X

[51] Dunlop, D.J., 2002. Theory and application of the Day plot (M_{rs}/M_s versus H_{cr}/H_c) 1. Theoretical curves and tests using titanomagnetites data. Journal of Geophysical Research: Solid Earth. 107(B3).
DOI: https://doi.org/10.1029/2001jb000486

[52] King, J., Banerjee, S.K., Marvin, J., et al., 1982. A comparison of different magnetic methods for determining the relative grain size of magnetite in natural materials: Some results from lake sediments. Earth and Planetary Science Letters. 59(2), 404–419.
DOI: https://doi.org/10.1016/0012-821X(82)90142-X

[53] Zhang, X., Li, X.L., Garzanti, E., et al., 2021. Sedimentary geochemistry response to climate change on a millennial timescale in the Qiantang River incised-valley system, eastern China. Chemical Geology. 586, 120587.
DOI: https://doi.org/10.1016/j.chemgeo.2021.120587

[54] Dankers, P., 1981. Relationship between median destructive field and remanent coercive forces for dispersed natural magnetite, titanomagnetite and hematite. Geophysical Journal International. 64(2), 447–461.
DOI: https://doi.org/10.1111/j.1365-246X.1981.tb02676.x

[55] Chaparro, M.A.E., Sinito, A.M., Bidegain, J.C., et al., 2006. Magnetic studies of natural goethite samples from Tharsis, Huelva, Spain. Geofísica Internacional. 45(4), 219–230.
DOI: https://doi.org/10.22201/igeof.00167169p.2006.45.4.159

[56] Özdemir, Ö., Dunlop, D.J., 2014. Hysteresis and coercivity of hematite. Journal of Geophysical Research: Solid Earth. 119(4), 2582–2594.
DOI: https://doi.org/10.1002/2013jb010739

[57] Ahmadzadeh, M., Romero, C., McCloy, J., 2017. Magnetic analysis of commercial hematite, magnetite, and their mixtures. AIP Advances, 8(5).
DOI: https://doi.org/10.1063/1.5006474

[58] Peters, C., Dekkers, M.J., 2003. Selected room temperature magnetic parameters as a function of mineralogy, concentration and grain size. Physics and Chemistry of the Earth, Parts A/B/C. 28(16–19), 659–667.
DOI: https://doi.org/10.1016/S1474-7065(03)00120-7

[59] Rosenbaum, J.G., Reynolds, R., Adam, D.P., et al., 1996. Record of Middle Pleistocene climate change from Buck Lake, Cascade Range, southern Oregon-Evidence from sediment magnetism, trace-element geochemistry, and pollen. Geological Society of America Bulletin. 108(10), 1328–1341.
DOI: https://doi.org/10.1130/0016-7606(1996)108<1328:ROMPCC>2.3.CO;2

[60] Sokol, E.V., Kozlikin, M.B., Kokh, S.N., et al., 2022. Phosphate Record in Pleistocene-Holocene Sediments from Denisova Cave: Formation Mechanisms and Archaeological Implications. Minerals. 12(5), 553.
DOI: https://doi.org/10.3390/min12050553

[61] Parker, A., 1970. An Index of Weathering for Silicate Rocks. Geological Magazine. 107(6), 501–504.
DOI: https://doi.org/10.1017/s0016756800058581

[62] Yang, S., Jung, H.S., Li, C., 2004. Two unique weathering regimes in the Changjiang and Huanghe drainage basins: geochemical evidence from river sediments. Sedimentary Geology. 164(1–2), 19–34.
DOI: https://doi.org/10.1016/j.sedgeo.2003.08.001

[63] Garzanti, E., Padoan, M., Setti, M., et al., 2014. Provenance versus weathering control on the composition of tropical river mud (southern Africa). Chemical Geology. 366, 61–74.
DOI: https://doi.org/10.1016/j.chemgeo.2013.12.016

[64] Kehl, M., Eckmeier, E., Franz, S.O., et al., 2014. Sediment sequence and site formation processes at the Arbreda Cave, NE Iberian Peninsula, and implications on human occupation and climate change during the Last Glacial. Climate of the Past. 10(5), 1673–1692.
DOI: https://doi.org/10.5194/cp-10-1673-2014

[65] Mora, G., Martínez, J.I., 2005. Sedimentary metal ratios in the Colombia Basin as indicators for water balance change in northern South America during the past 400.000 years. Paleoceanography. 20(4).
DOI: https://doi.org/10.1029/2005pa001132

[66] Gehring, A.U., Fischer, H., Louvel, M., et al., 2009.

High temperature stability of natural maghemite: a magnetic and spectroscopic study. Geophysical Journal International. 179(3), 1361–1371. DOI: https://doi.org/10.1111/j.1365-246x.2009.04348.x

[67] Jordanova, N., 2017. Soil magnetism: Applications in Pedology, Environmental Science and Agriculture. Academic Press: UK.

[68] Rankey, E.C., Farr, M.R. 1997. Preserved pedogenic mineral magnetic signature, pedogenesis, paleoclimate change: Pennsylvanian Roca Shale (Virgilian, Asselian), central Kansas, USA. Sedimentary Geology. 114(1–4), 11–32. DOI: https://doi.org/10.1016/S0037-0738(97)00102-4

[69] Maher, B.A., Karloukovski, V.V., Mutch, T.J., 2004. High-field remanence properties of synthetic and natural submicrometre haematites and goethites: significance for environmental contexts. Earth and Planetary Science Letters. 226(3–4), 491–505. DOI: https://doi.org/10.1016/j.epsl.2004.05.042

[70] Tămaş, T., Kristály, F., Barbu-Tudoran, L., 2011. Mineralogy of Iza Cave (Rodnei Mountains, N. Romania). International Journal of Speleology. 40(2), 171–179. DOI: https://doi.org/10.5038/1827-806x.40.2.9

[71] Maher, B.A., 1988. Magnetic properties of some synthetic sub-micron magnetites. Geophysical Journal International. 94(1), 83–96. DOI: https://doi.org/10.1111/j.1365-246x.1988.tb03429.x

[72] Evans, M.E., Heller, F., 2003. Environmental magnetism: Principles and Applications of Enviromagnetics. Academic Press: USA. DOI: https://doi.org/10.1016/j.quascirev.2004.05.004

[73] Casey, T., 2009. Iron and manganese in water. Aquavarra Research R&D Publications. Paper 3.

[74] Usman, U.A., Yusoff, I., Raoov, M., et al., 2021. Natural sources of iron and manganese in groundwater of the lower Kelantan River Basin, North-eastern coast of Peninsula Malaysia: water quality assessment and an adsorption-based method for remediation. Environmental Earth Sciences. 80(12), 425. DOI: https://doi.org/10.1007/s12665-021-09717-0

[75] Torrent, J., Guzman, R., 1982. Crystallization of Fe(III)-Oxides from ferrihydrite in salt solutions: osmotic and specific ion effects. Clay Minerals. 17(4), 463–469. DOI: https://doi.org/10.1180/claymin.1982.017.4.09

[76] Maher, B., 1986. Characterisation of soils by mineral magnetic measurements. Physics of the Earth and Planetary Interiors. 42(1–2), 76–92. DOI: https://doi.org/10.1016/S0031-9201(86)80010-3

[77] Maher, B.A., Thompson, R., 1995. Paleoclimatic significance of the mineral magnetic record of the Chinese loess and paleosols. Quaternary Research. 37(2), 155–170. DOI: https://doi.org/10.1016/0033-5894(92)90079-X

[78] Shahack-Gross, R., Berna, F., Karkanas, P., et al., 2004. Bat guano and preservation of archaeological remains in cave sites. Journal of Archaeological Science. 31(9), 1259–1272. DOI: https://doi.org/10.1016/j.jas.2004.02.004

[79] Dumitraş, D.G., Marincea, Ş., Fransolet, A.M., 2004. Brushite in the bat guano deposit from the "dry" Cioclovina Cave (Sureanu Mountains, Romania). Neues Jahrbuch Für Mineralogie, Abhandlungen. 180(1), 45–64. DOI: https://doi.org/10.1127/0077-7757/2004/0180-0045